

ORIGINAL ARTICLE

Open Access



# Oblique Cutting Based Mechanical Model for Insertion Torque of Dental Implant

Luli Li<sup>1,2</sup>, Song Zhang<sup>1,2\*</sup> , Quhao Li<sup>1,2</sup>, Cuirong Bian<sup>3</sup> and Airong Zhang<sup>1,2</sup>

## Abstract

The insertion torque of a dental implant is an important indicator for the primary stability of dental implants. Thus, the preoperative prediction for the insertion torque is crucial to improve the success rate of implantation surgery. In this present research, an alternative method for prediction of implant torque was proposed. First, the mechanical model for the insertion torque was established based on an oblique cutting process. In the proposed mechanical model, three factors, including bone quality, implant geometry and surgical methods were considered in terms of bone-quality coefficients, chip load and insertion speeds, respectively. Then, the defined bone-quality coefficients for cancellous bone with the computed tomography (CT) value of 235–245, 345–355 and 415–425 Hu were obtained by a series of insertion experiments of IS and ITI implants. Finally, the insertion experiments of DIO implants were carried out to verify the accuracy of developed model. The predicted insertion torques calculated by the mechanical model were compared with those acquired by insertion experiments, with good agreement, the relative error being less than 15%. This method allows the insertion torque for different implant types to be quickly established and enhances prediction accuracy by considering the effects of implants' geometries and surgical methods.

**Keywords:** Insertion torque, Mechanical model, Oblique cutting, Dental implant

## 1 Introduction

Implant dentures have been one of the most popular options for teeth loss in last decade [1]. After the implant socket is prepared by a series of processes such as drilling, reaming and tapping, the implant is inserted in alveolar bone with a certain torque, which called the insertion torque. Most clinical data shows that 30–70 N·cm is a reasonable range of insertion torque to achieve satisfactory initial implant stability. This means that if the insertion torque for the implant is in this range, it would ideally be considered that the surgery would be successful [2–4], otherwise, the surgery would fail. As the insertion torque can only be known after the whole implant is inserted, if the insertion torque is not good (lower than 30 N·cm or higher than 70 N·cm), the patient has to

endure a second surgery. However, if the insertion torque could be predicted before the surgery, it would allow the dentist to make or adjust the surgery plan and improve the surgery success rate. So, this research focuses on the preoperative prediction of the insertion torque. Actually, the reasonable range of insertion torque is different for each patient, depending on their age, gender and height [5, 6], and also implant shape and diameter [7, 8], loading condition [9], etc. However, it is supposed here that the 30–70 N·cm is reasonable for any condition.

To predict implant insertion torque, three factors, implant geometries [10], surgical methods [11, 12] and bone quality, have been considered. It has been shown that the larger insertion torque can be obtained by a conical [13], large-diameter implant [14] or a small-diameter implant socket [15, 16]. Bone quality, which is primarily influenced by bone density, is a key focus for dentists in-clinic, and has been shown to be positively correlated with insertion torque [17]. Computed tomography (CT) is normally used to quantify bone density in-clinic and

\*Correspondence: [zhangsong@sdu.edu.cn](mailto:zhangsong@sdu.edu.cn)

<sup>1</sup> School of Mechanical Engineering, Shandong University, Jinan 250061, China

Full list of author information is available at the end of the article

several empirical fits have been established for the linear relationship between CT value and insertion torque, which were further used to predict the insertion torque [18–21]. The accuracy of these empirical fits is largely high, (greater than 80%), however, these formulas are only suitable for just one combination of implant and method of surgery. In order to use empirical formulas to predict the insertion torque, formulas for every combination of implants and surgery would have to be established, which would be time-consuming and expensive.

In this research, an alternative method to predict the insertion torque is provided by establishing a mechanical model based on oblique cutting theory, although it has been widely accepted in engineering, has not previously been used in calculating insertion torque for dental implants. In the proposed model, using DIO implants as an example, the effects of implant geometry and surgical methods were captured by chip load and insertion speeds, respectively, meanwhile the effect of bone quality was considered by the defined coefficients, termed bone-quality coefficients. Then, the bone-quality coefficients for the bone quality with CT value of 235–245, 345–355 and 415–425 Hu were obtained by a series of insertion experiments using the IS and ITI implants. With the obtained coefficients, a relationship between insertion torque and bone quality was obtained. Then, the DIO implants were used to verify the accuracy of the developed model. The results show that the model has high accuracy with relative error less than 15%.

## 2 Mechanical Model Based on Oblique Cutting Theory

The insertion process for dental implants involves two forming methods, i.e., the thread-cutting process [22] for implants with cutting edges and the thread-forming process for implants without cutting edges [23]. In this section, the implant typed DIO SFR5010 (DIO Innovation Health Care, Busan City, Korea) with 4 cutting edges in the apical part and continuous threads in the tail part was selected to establish the mechanical model for insertion torque.

### 2.1 Forming Process of Matching Threads

Figure 1 describes the geometry of DIO SFR5010 and its insertion process, where Figure 1(a) is the initial position of implant while Figure 1(b) is the position after one thread was inserted. The threads in the bone are initially formed by successive passes of the cutting edges in the apical part of the implant, in a similar operation to thread-cutting using a tap. This process is called the thread-cutting process, and the bone debris generate in this process. The threads in the tail part of the implant,

without cutting edges, are subsequently inserted [24], in what is called the thread-forming process without bone debris generation.

To detail the shape of the matching threads, DIO SFR5010 was cut into 12 thin slices considering only one thread in each. In the apical part, each slice was further separated into 4 cutting elements by 4 cutting edges. The whole process was separated into 12 steps, with one thread inserted into the implant socket per step. The shape of the matching threads in each step was defined by the cutting element passed last. A global coordinate system  $\{C:OXYZ\}$  was attached to the implant. Its origin point  $O$  was the starting point of the first threads, and its  $Z$ -axis was set along the axis of rotation. The cutting element coordinate system  $\{c:oxyz_i\}$  was given to each cutting element. Its  $x$ -axis was set parallel to the helical path, where  $i$  indicates the  $i$ th thread.

The helical path of the matching thread is the same as that of the implant threads, and can be expressed as follows:

$$g(P, \theta) = \begin{cases} x(P, \theta) = (P\theta/2\pi \tan \beta + b + h_d) \cdot \cos \theta, \\ y(P, \theta) = (P\theta/2\pi \tan \beta + b + h_d) \cdot \sin \theta, \\ z(P, \theta) = P\theta/2\pi, \end{cases}$$

$x, y, z$  are the point coordinates of the helical path;  $\theta$  is the angular position of the helical path;  $b, h_d, P$  and  $\beta$  are the initial radius, tooth height, pitch and taper angle of DIO SFR5010, respectively. Particularly, in the tail part,  $\beta = 0$ .

The radius  $r_i$  of the matching thread can be given by the radial distance from the  $Z$ -axis to the outer geometry of the  $i$ th thread as:

$$r_i = \sqrt{x(P, \theta_i)^2 + y(P, \theta_i)^2}. \quad (2)$$

The engagement  $h_i$  of the  $i$ th cutting element can be calculated as follows:

$$h_i = r_i(P, \theta_i) - r_i(P, \theta_i - \theta_{i-1}), \quad (3)$$

$\theta_{i-1}$  is the angular position of the last cutting element.

The thread inclination angle  $\gamma$  can be calculated as follows:

$$\gamma = \pi/2 + \xi - \lambda = \pi/2 + \arctan(P/2\pi r_i) - \lambda, \quad (4)$$

where,  $\xi$  and  $\lambda$  are the thread lead angle and the flute helix angle, respectively.

### 2.2 Force–chip Load Relationship

Three assumptions were made as follows: ① each cutting element sustains normal and friction forces, and all forces are applied on the centroid of the respective faces; ② the

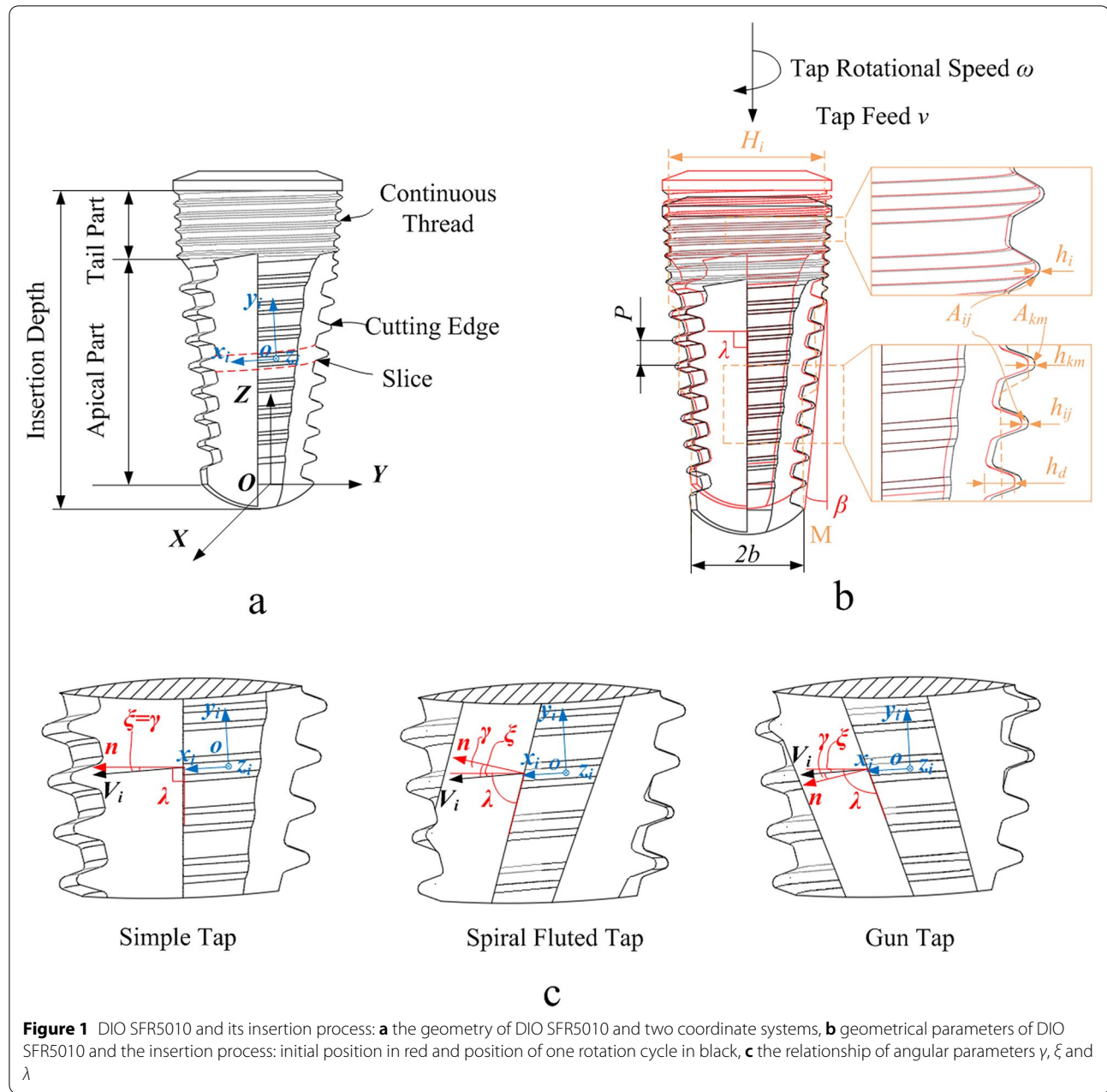


**Figure 1** DIO SFR5010 and its insertion process: **a** the geometry of DIO SFR5010 and two coordinate systems, **b** geometrical parameters of DIO SFR5010 and the insertion process: initial position in red and position of one rotation cycle in black, **c** the relationship of angular parameters  $\gamma$ ,  $\xi$  and  $\lambda$

effects of elastic recovery for the prediction of insertion torque were ignored; ③ insertion torques generated by one thread remained constant throughout the whole insertion process.

According to these assumptions, the forces applied on all cutting elements can be composed of the normal force  $F_n$  and the friction force  $F_f$  as follows [25]:

$$F_n = K_n A, \quad (5)$$

$$F_f = K_f A, \quad (6)$$

$A$  is chip load, which is equal to the unformed chip area and depends on the implant geometry;  $K_n$  and  $K_f$  are specific energies, which are related to the tool geometry and work conditions as follows [26]:

$$\ln K_n = a_0 + a_1 \ln h + a_2 \ln V + a_3 \ln h \ln V, \quad (7)$$

$$\ln K_f = b_0 + b_1 \ln h + b_2 \ln V + b_3 \ln h \ln V, \quad (8)$$

$V$  is the insertion speed,  $h$  is the radial engagement of each cutting element, and  $a_0$ – $a_3$  and  $b_0$ – $b_3$  are the

specific energy coefficients which depend on materials of the cutting tool (i.e., implant) and the workpiece (i.e., cancellous bone). As most implants are composed of titanium or titanium-alloys, the  $a_0$ – $a_3$  and  $b_0$ – $b_3$  were only determined by bone quality and defined as bone-quality coefficients.

Considering the normal force  $F_n$  and the friction force  $F_f$  are different during thread-cutting and thread-forming processes, they are discussed in Sections 2.2.1 and 2.2.2, respectively.

### 2.2.1 Forces in Thread-cutting Process

In the thread-cutting process, as the cutting velocity and the chip flow directions are not perpendicular to the cutting edge, this can be considered an oblique cutting process [27, 28] as shown in Figure 2. The coordinate system  $\{c:ox,y,z\}$  is used to define the forces on each elements during thread-cutting process. Two planes, the normal and chip-flow plane, were introduced. The normal plane was defined by the  $x_i$ -axis and  $z_i$ -axis and the chip-flow plane was coincident with the rake surface of the cutting edges. In the normal plane, the normal force  $F_{cni}$  was defined perpendicular to the rake surface. In the chip-flow plane, the friction force  $F_{cfi}$  was defined collinear with the chip-flow orientation [29]. Meanwhile, the chip-flow angle  $i$  was defined equal to the inclination angle  $\gamma$  based on the Stabler's rule.

According to Eqs. (5) and (6),  $F_{cni}$  and  $F_{cfi}$  can be expressed as follows:

$$F_{cni} = K_{cn} A_{ci}, \quad (9)$$

$$F_{cfi} = K_{cf} A_{ci}, \quad (10)$$

where,  $A_{ci}$  are the chip load of the  $i$ th cutting element, and  $K_{cn}$  and  $K_{cf}$  are the specific energies in the thread-cutting

process. According to Eqs. (7) and (8), these can be calculated as:

$$\ln K_{cn} = a_0 + a_1 \ln h_i + a_2 \ln V_i + a_3 \ln h_i \ln V_i, \quad (11)$$

$$\ln K_{cf} = b_0 + b_1 \ln h_i + b_2 \ln V_i + b_3 \ln h_i \ln V_i, \quad (12)$$

where,  $a_0$ – $a_3$  and  $b_0$ – $b_3$  are the bone-quality coefficients during the thread-cutting processes, to be further determined by insertion experiments.

The chip load  $A_{ci}$  can be calculated as follows:

$$A_{ci} = h_i(w_i + 2h_i \tan \alpha_1 + 2h_i \tan \alpha_2), \quad (13)$$

where,  $w$  is the tooth top width of  $i$ th cutting element, the radial engagement  $h_i$  can be calculated according to Eq. (3) as:

$$h_i = r_i(P, \theta_i) - r_i(P, \theta_i - 2\pi/N_t), \quad (14)$$

where,  $N_t$  is the number of cutting edges. For DIO SFR5010,  $N_t = 4$ .

By decomposing  $F_{cni}$  and  $F_{cfi}$  into the three axes of  $\{c:ox,y,z\}$ , three axial forces  $F_{xi}$ ,  $F_{yi}$  and  $F_{zi}$  can be obtained as follows:

$$\begin{pmatrix} F_{xi} \\ F_{yi} \\ F_{zi} \end{pmatrix} = \begin{pmatrix} \cos \varphi \\ 0 \\ -\sin \varphi \end{pmatrix} F_{cni} + \begin{pmatrix} -\sin \varphi \\ \sin \gamma \\ \cos \gamma \cos \varphi \end{pmatrix} F_{cfi}. \quad (15)$$

Then, the thrust force  $F_{thri}$  and tangential force  $F_{tani}$  of each cutting element and the total insertion torque  $M$  can be calculated from Eqs. (16)–(18), respectively.

$$F_{tani} = F_{xi} \cos \xi + F_{yi} \sin \xi, \quad (16)$$

$$F_{thri} = F_{yi} \cos \xi - F_{xi} \sin \xi, \quad (17)$$

$$M = \sum_{i=1}^n F_{tani} \cdot r_i. \quad (18)$$

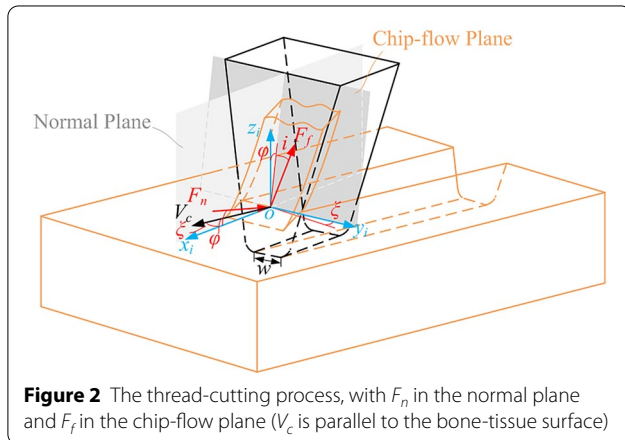


**Figure 2** The thread-cutting process, with  $F_n$  in the normal plane and  $F_f$  in the chip-flow plane ( $V_c$  is parallel to the bone-tissue surface)

### 2.2.2 Forces in Thread-forming Process

Like the thread-cutting process, in the thread-forming process, the cutting velocity and the chip flow directions are not perpendicular either. Therefore, the model was also based on oblique cutting (forming).

However, in this process, as previously mentioned, there is no cutting process, the matching thread is formed by bone plastic deformation and flow. To define the forces during the thread-forming process, six faces named  $S_1$ – $S_6$  were introduced as shown in Figure 3. The highest portion of the implant edge, defined by  $S_4$ – $S_6$ ,

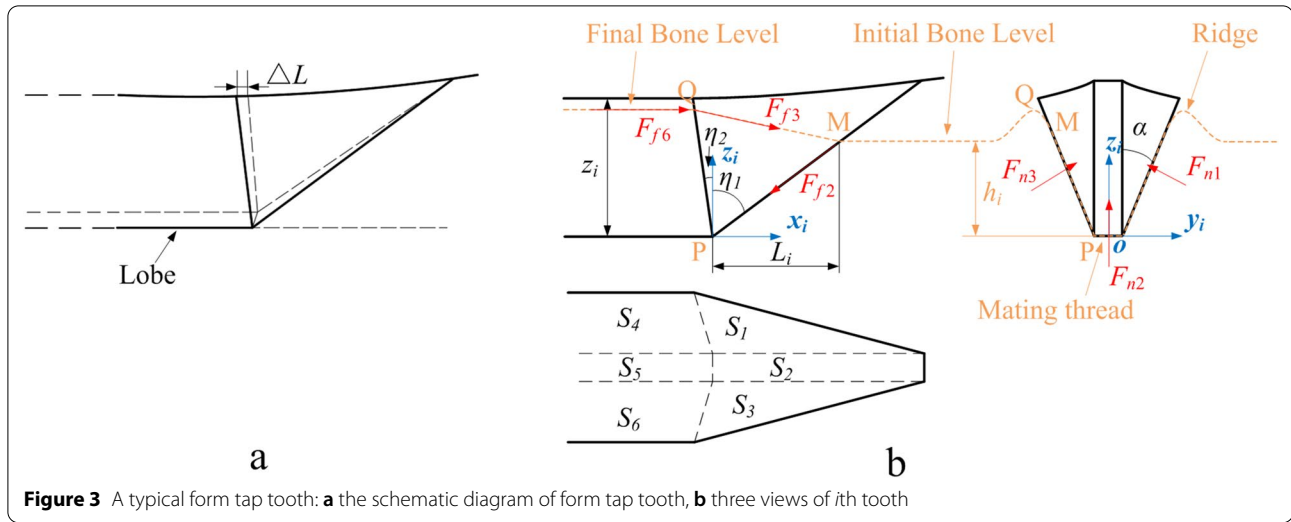


**Figure 3** A typical form tap tooth: **a** the schematic diagram of form tap tooth, **b** three views of  $i$ th tooth

was named as the lobe. This defines the final geometry of the matching thread. The regions before the lobe have a slope to provide relief, which was used to minimize the contact between the implant and the bone material. The normal forces  $F_{ni}$  were defined proportional to the contact areas, and the friction forces  $F_{fi}$  were defined collinear with chip-flow orientation [30], in the same way as the thread-cutting process:

$$F_{fi} = K_{fi} A_{fi}, \quad (19)$$

$$F_{fi} = K_{ff} A_{fi}, \quad (20)$$

where,  $K_{fi}$  and  $K_{ff}$  are the specific energies during the thread-forming process. According to the Eqs. (7) and (8), they can be calculated using:

$$\ln K_{fi} = c_0 + c_1 \ln h_i + c_2 \ln V_i + c_3 \ln h_i \ln V_i, \quad (21)$$

$$\ln K_{ff} = d_0 + d_1 \ln h_i + d_2 \ln V_i + d_3 \ln h_i \ln V_i, \quad (22)$$

where,  $c_0$ – $c_3$  and  $d_0$ – $d_3$  are the bone-quality coefficients in the thread-forming process which would be further determined by insertion experiments.

The chip load  $A_{fi}$  can be calculated as follows:

$$A_{fi} = \begin{cases} S_1 = S_3 = |\mathbf{PQ} \times \mathbf{PM}|/2 = h_i \cdot z_i \cdot y(\eta)/2, \\ S_2 = w \cdot h_i / \cos \eta_1, \end{cases} \quad (23)$$

$$y(\eta) = \sqrt{(\tan \alpha)^2 + (\tan \eta_1 \tan \alpha)^2 + (\tan \eta_1 + \tan \eta_2)^2}, \quad (24)$$

where,  $h_i$  is the radial engagement of the  $i$ th thread and it was given by Eq. (3),  $\alpha$  is the thread angle,  $\eta_1$  and  $\eta_2$  are the incident angle and the lobe-relief angle of threads,

respectively,  $z_i$  is the  $z$  coordinate of the point  $Q$  and it is given by:

$$z_i = \sum_{n=1}^i h_i = r_i(P, \theta_i) - r_k(P_k, \theta_k), \quad (25)$$

where,  $r_k$  is the first thread without cutting edges.

By decomposing  $F_{fi}$  and  $F_{ff}$  of the  $i$ th thread into three axes of  $\{c:ox_iy_iz_i\}$ , three axial forces can be obtained by:

$$\begin{pmatrix} F_{xi} \\ F_{yi} \\ F_{zi} \end{pmatrix} = \begin{pmatrix} -\cos \eta_1 \\ 0 \\ \sin \eta_1 \end{pmatrix} F_{fi} + \begin{pmatrix} \sin \eta_1 \\ 0 \\ \cos \eta_1 \end{pmatrix} F_{ff}. \quad (26)$$

Then, the thrust force  $F_{thri}$  and the tangential force  $F_{tani}$  of each cutting element and the total insertion torque  $M$  can be calculated by:

$$F_{tani} = F_{xi} \cos \xi + F_{yi} \sin \xi, \quad (27)$$

$$F_{thri} = F_{yi} \cos \xi - F_{xi} \sin \xi, \quad (28)$$

$$M = \sum_{i=1}^n F_{tani} \cdot r_i. \quad (29)$$

According to Eqs. (15)–(18) and (26)–(29), it could be observed that the insertion torque was related to the normal and the friction force, which were determined by ① bone-quality coefficients, ② insertion speed  $V$ , ③ radial engagement  $h_i$  and ④ chip load  $A$ . These give a good explanation for the effects of the bone quality, surgical methods, and the implant geometry, respectively. When the implant and the surgical method were selected,  $h_i$ ,  $A$



and  $V$  can be determined. The only consideration is the bone-quality coefficients, which were given in Section 3.

### 3 Determination of Bone-quality Coefficient and Validation of Mechanical Model

To define the bone-quality coefficients, more than 80 bone blocks with the size of  $25 \times 25 \times 40 \text{ mm}^3$  were cut from the epiphysis areas of four bovine femurs with different age, weight and gender as shown in Figure 4. The mean CT value of bone material within 1 mm around the predicted implant socket for each bone block as shown in Table 1 were recorded by Planmeca ProMax® 3D Mid CT (Planmeca UK Limited, Coventry, UK. scanning time: 13.929 s, tube voltage: 90 kV tube current: 10 mA). According to recorded CT value, 36 bone blocks were selected and further classified into 3 groups with the CT value of 235–245, 345–355, and 415–425 HU, respectively.

#### 3.1 Insertion Experiments

Three groups of insertion experiments were conducted. The geometry parameters of these implants were shown as Table 2.

In Table 2,  $\beta_1$ ,  $\alpha_1$ ,  $L_1$ ,  $D_1$ ,  $P_1$ ,  $H_1$  are the parameters of apical part of implant DIO SFR5010 while  $\beta_2$ ,  $\alpha_2$ ,  $\alpha_3$ ,  $L_2$ ,  $D_2$ ,  $P_2$ ,  $H_2$  the tail part of implant DIO SFR5010.

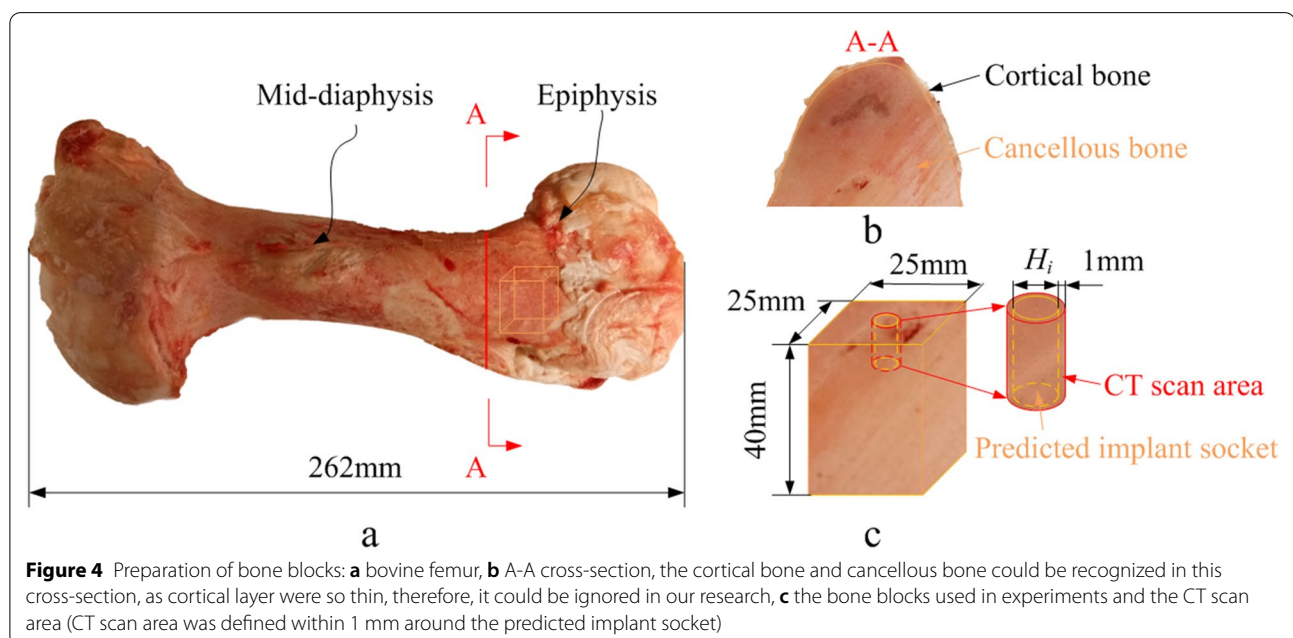
IS implants (IS BIS4510 and IS BIS5010, Neobiotech Co.,Ltd., Seoul, Korea) with cutting edges were used to determine bone-quality coefficients  $a_0$ – $a_3$  and  $b_0$ – $b_3$  while ITI implants (ITI RN4510 and ITI RN5010, ITI International Team for Implantology, Basel, Switzerland)

**Table 1** CT value of 3 group bone blocks




Group 1	CT (Hu)	Group 2	CT (Hu)	Group 3	CT (Hu)
A <sub>01</sub>	237.60	B <sub>01</sub>	354.86	C <sub>01</sub>	418.48
A <sub>02</sub>	241.54	B <sub>02</sub>	345.35	C <sub>02</sub>	419.58
A <sub>03</sub>	236.42	B <sub>03</sub>	352.68	C <sub>03</sub>	417.99
A <sub>04</sub>	237.08	B <sub>04</sub>	346.42	C <sub>04</sub>	422.54
A <sub>05</sub>	242.13	B <sub>05</sub>	348.57	C <sub>05</sub>	420.26
A <sub>06</sub>	239.56	B <sub>06</sub>	353.63	C <sub>06</sub>	421.41
A <sub>07</sub>	241.69	B <sub>07</sub>	349.21	C <sub>07</sub>	417.69
A <sub>08</sub>	235.69	B <sub>08</sub>	350.96	C <sub>08</sub>	423.93
A <sub>09</sub>	237.72	B <sub>09</sub>	354.12	C <sub>09</sub>	415.34
A <sub>10</sub>	240.34	B <sub>10</sub>	348.56	C <sub>10</sub>	419.47
A <sub>11</sub>	237.32	B <sub>11</sub>	350.12	C <sub>11</sub>	416.95
A <sub>12</sub>	241.80	B <sub>12</sub>	349.61	C <sub>12</sub>	424.01
Range	235–245	Range	345–355	Range	415–425

without cutting edges were used to determine bone-quality coefficients  $c_0$ – $c_3$  and  $d_0$ – $d_3$ . DIO SFR5010 were used to verify the established model.

The insertion experiments involved the drilling processes of implant sockets and the insertion process of implants. They were conducted on the CNC machine (HAAS OM-2A, Haas Automation Inc., Oxnard, CA, USA). The equipment setting was shown in Figure 5. The parameters of drills and experiment setting were listed as Table 3. To minimize the coaxially error between the implants and corresponding predicted implant sockets, there was no interruption between the drilling and insertion processes. The high accuracy



**Table 2** Implant parameters

Implant	Appearance	Angle (°)	Size (mm)
IS BIS4510		$\beta_1=1.0$ $\beta_2=17$ $\alpha_1=6$ $\alpha_2=30$ $\lambda=90$ $\varphi=0$	$L=10$ $D=\varphi 4.5$ $P=0.8$ $h_d=0.25$ $w=0.08$ $H=\varphi 4.4$
IS BIS5010		$\beta_1=1.7$ $\beta_2=17$ $\alpha_1=6$ $\alpha_2=30$ $\lambda=90$ $\varphi=0$	$L=10$ $D=\varphi 5$ $P=0.8$ $h_d=0.25$ $w=0.08$ $H=\varphi 4.9$
ITI RN4210		$\beta=0$ $\alpha=30$ $\eta_1=85$ $\eta_2=10$ $\xi=4.74$	$L=10$ $D=\varphi 4.8$ $P=1.25$ $H=\varphi 4.2$ $w=0.1$

dynamometer (Kistler9119AA2, Kistler Instruments Ltd., London, UK, sampling rate: 1200 Hz) was used to capture the thrust forces and insertion torques during the insertion process of implants.

### 3.2 Bone-quality Coefficients

The results of thrust forces  $F_{thri}$  and insertion torques of IS and ITI implants were presented as Figure 6.

The peak torque and thrust force were used to determine the bone-quality coefficients for thread-cutting and

**Table 2** (continued)

Implant	Appearance	Angle (°)	Size (mm)
ITI RN4810		$\beta=0$ $\alpha=30$ $\eta_1=85$ $\eta_2=10$ $\xi=4.74$	$L=10$ $D=\varphi 4.8$ $P=1.25$ $H=\varphi 4.2$ $w=0.1$
DIO SFR5010		$\beta_1=0$ $\alpha_1=8.5$ $\eta_1=85$ $\eta_2=10$ $\xi=1.5$ $\beta_2=8.75$ $\alpha_2=7$ $\alpha_3=30$ $\lambda=90$ $\varphi=0$	$L_1=2.5$ $D_1=\varphi 5.0$ $P_1=0.4$ $H_1=\varphi 4.9$ $w_1=0.05$ $L_2=6.5$ $D_2=\varphi 5$ $P_2=0.8$ $H_2=\varphi 4.2$ $w_2=0.12$

thread-forming processes. The obtained bone-quality coefficients were listed in Tables 4 and 5.

It was observed that the bone-quality coefficients  $a_0-a_3$ ,  $b_0-b_3$ ,  $c_0-c_3$  and  $d_0-d_3$  were different in 3 group, which is the good explanation for the effects of bone quality.

Until now, we can get the general equations for dentists to predict insertion torque by substituting the bone-quality coefficients into the mathematical framework. Taking Group 1 as an example,  $K_{cn}$ ,  $K_{cf}$ ,  $K_{fn}$  and  $K_{ff}$  were given by:

$$K_{cn} = e^{14.6} \cdot h^{0.17} \cdot V^{0.44}, \quad (30)$$

$$K_{cf} = e^{12.9} \cdot h^{0.02} \cdot V^{0.17}, \quad (31)$$

$$K_{fn} = e^{22.4} \cdot h^{0.06} \cdot V^{0.16}, \quad (32)$$

$$K_{ff} = e^{21.2} \cdot h^{0.06} \cdot V^{0.15}. \quad (33)$$

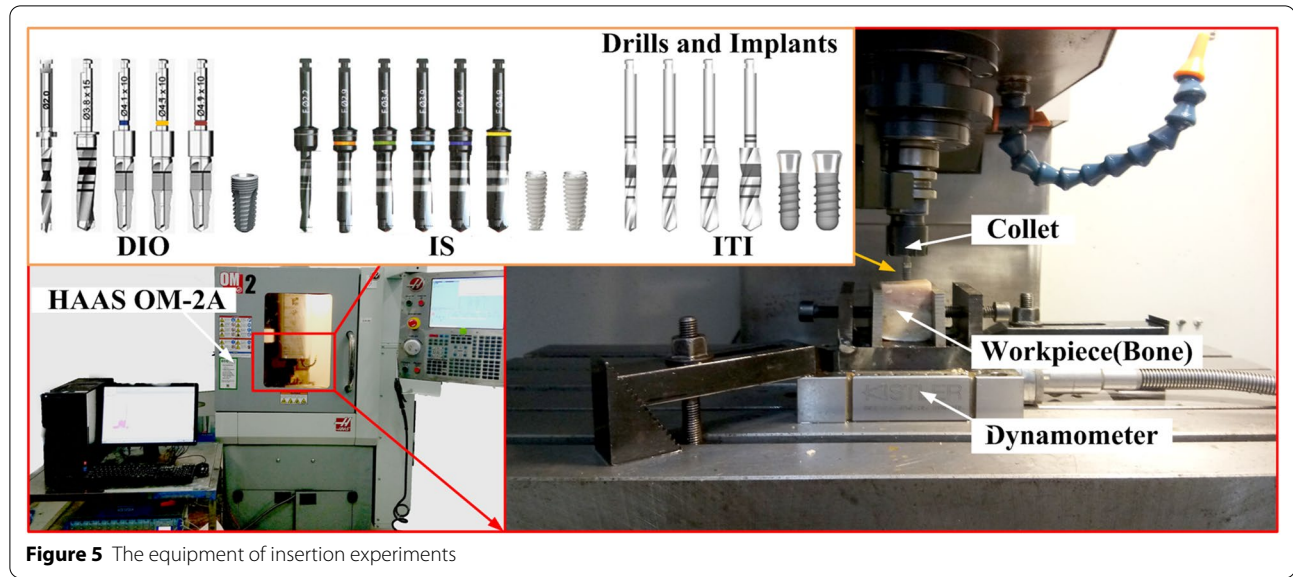


**Figure 5** The equipment of insertion experiments

As the  $K_{cf}$  is much smaller than  $K_{cn}$ , it can be ignored, and insertion torque with simplified form can be given by:

$$M = e^{14.6} \cos \xi \cos \varphi \cdot V^{0.44} \sum_{i=1}^n r_i h_i^{2.17} (\tan \alpha_1 + \tan \alpha_2), \quad (34)$$

$$M = y(\eta) \cos \xi \sum_{i=1}^n z_i r_i h_i (\sin \eta_1 e^{21.2} V^{0.15} - \cos \eta_1 e^{22.4} V^{0.16}), \quad (35)$$

where Eq. (34) is used for implant with cutting edge while Eq. (35) is used for implant without cutting edge,  $y(\eta)$  and  $z_i$  are given as follows:

$$y(\eta) = \sqrt{(\tan \alpha)^2 + (\tan \eta_1 \tan \alpha)^2 + (\tan \eta_1 + \tan \eta_2)^2}, \quad (36)$$

$$z_i = \sum_{n=1}^i h_i = r_i - r_1. \quad (37)$$

### 3.3 Validation of Mechanical Model

The predicted insertion torque of bone block  $A_{11}$ ,  $A_{12}$ ,  $B_{11}$ ,  $B_{12}$ ,  $C_{11}$ ,  $C_{12}$  were compared with that obtained by insertion experiments using DIO SFR5010. The torques of each thread during the insertion processes were listed in Figure 7 and Table 6. The insertion torque is the peak torque. As the bone blocks  $A_{11}$  and  $A_{12}$  are both in Group 1, thus, they share the same bone-quality in either thread-cutting or thread forming process, and there is only one predicted value to be compared, same as  $B_{11}$  and  $B_{12}$ ,  $C_{11}$  and  $C_{12}$ .

In Figure 7 and Table 6, the two series of measured values for Group 1–3 were obtained by insertion experiments by bone blocks  $A_{11}$ ,  $A_{12}$ ,  $B_{11}$ ,  $B_{12}$ ,  $C_{11}$ ,  $C_{12}$ , respectively. As shown in Figure 7, the variations of material properties of bone blocks brought a significant fluctuation of the initial insertion torques obtained by experiments. But the trends and predicted peak insertion torques by mechanical models agreed well with that acquired by insertion experiments. The relative errors were calculated as follows.

$$\left| \frac{T_{pred} - T_{measured}}{T_{measured}} \right| \times 100\%. \quad (38)$$

The errors were mainly caused by ① the simplification in the modeling process; ② the deviation between the predicted implant sockets and the real implant sockets. As the surgery process for implant socket is fully conducted by dentist, the real implant sockets could not perfect as predicted one. There would be, for example, the deviation for position or the central axis even for a skilled dentist; ③ the heterogeneous of bone quality in CT scan area. As the material properties for bone material does not only depend on the bone density, but it also depends on the microstructure of the trabecular bone, the unit of the cancellous bone. As the microstructure of the trabecular bone is complex and different from point to point, there is high heterogeneous properties for bone material. In prediction model, the material properties of bone are decided by bone density, therefore, the effect of the heterogeneous cannot be predicted. We think, the error within 15% could be accepted in clinical prediction. In addition, considering the errors were contributed



**Table 3** Parameters of insertion experiments

Drills and Implants types	Bone blocks No.	Diameter $d$ (mm)	Insertion speed $\omega$ (r/min)	Feed rate $v$ (mm/min)
IS TSD22F	A <sub>01</sub> -A <sub>02</sub> ; B <sub>01</sub> -B <sub>02</sub> ; C <sub>01</sub> -C <sub>02</sub>	2.2	1200	10
IS TSD29F	A <sub>01</sub> -A <sub>02</sub> ; B <sub>01</sub> -B <sub>02</sub> ; C <sub>01</sub> -C <sub>02</sub>	2.9	1200	10
IS TSD34F	A <sub>01</sub> -A <sub>02</sub> ; B <sub>01</sub> -B <sub>02</sub> ; C <sub>01</sub> -C <sub>02</sub>	3.4	1200	10
IS TSD39F	A <sub>01</sub> -A <sub>02</sub> ; B <sub>01</sub> -B <sub>02</sub> ; C <sub>01</sub> -C <sub>02</sub>	3.9	1000	10
IS TSD44F	A <sub>01</sub> -A <sub>02</sub> ; B <sub>01</sub> -B <sub>02</sub> ; C <sub>01</sub> -C <sub>02</sub>	4.4	800	10
IS BIS4510	A <sub>01</sub> ; B <sub>01</sub> ; C <sub>01</sub>	4.5	20	16
IS BIS4510	A <sub>02</sub> ; B <sub>02</sub> ; C <sub>02</sub>	4.5	30	24
IS TSD22F	A <sub>03</sub> -A <sub>05</sub> ; B <sub>03</sub> -B <sub>05</sub> ; C <sub>03</sub> -C <sub>05</sub>	2.2	1200	10
IS TSD29F	A <sub>03</sub> -A <sub>05</sub> ; B <sub>03</sub> -B <sub>05</sub> ; C <sub>03</sub> -C <sub>05</sub>	2.9	1200	10
IS TSD34F	A <sub>03</sub> -A <sub>05</sub> ; B <sub>03</sub> -B <sub>05</sub> ; C <sub>03</sub> -C <sub>05</sub>	3.4	1200	10
IS TSD39F	A <sub>03</sub> -A <sub>05</sub> ; B <sub>03</sub> -B <sub>05</sub> ; C <sub>03</sub> -C <sub>05</sub>	3.9	1000	10
IS TSD44F	A <sub>03</sub> -A <sub>05</sub> ; B <sub>03</sub> -B <sub>05</sub> ; C <sub>03</sub> -C <sub>05</sub>	4.4	1000	10
IS TSD49F	A <sub>03</sub> -A <sub>05</sub> ; B <sub>03</sub> -B <sub>05</sub> ; C <sub>03</sub> -C <sub>05</sub>	4.9	800	10
IS BIS5010	A <sub>03</sub> ; B <sub>03</sub> ; C <sub>03</sub>	5.0	20	16
IS BIS5010	A <sub>04</sub> -A <sub>05</sub> ; B <sub>04</sub> -B <sub>05</sub> ; C <sub>04</sub> -C <sub>05</sub>	5.0	30	24
ITI 044.210	A <sub>06</sub> -A <sub>07</sub> ; B <sub>06</sub> -B <sub>07</sub> ; C <sub>06</sub> -C <sub>07</sub>	2.2	800	10
ITI 044.214	A <sub>06</sub> -A <sub>07</sub> ; B <sub>06</sub> -B <sub>07</sub> ; C <sub>06</sub> -C <sub>07</sub>	2.8	600	10
ITI 044.250	A <sub>06</sub> -A <sub>07</sub> ; B <sub>06</sub> -B <sub>07</sub> ; C <sub>06</sub> -C <sub>07</sub>	3.5	500	10
ITI RN4110	A <sub>06</sub> ; B <sub>06</sub> ; C <sub>06</sub>	4.1	12	15
ITI RN4110	A <sub>07</sub> ; B <sub>07</sub> ; C <sub>07</sub>	4.1	15	18.75
ITI 044.210	A <sub>08</sub> -A <sub>10</sub> ; B <sub>08</sub> -B <sub>10</sub> ; C <sub>08</sub> -C <sub>10</sub>	2.2	800	10
ITI 044.214	A <sub>08</sub> -A <sub>10</sub> ; B <sub>08</sub> -B <sub>10</sub> ; C <sub>08</sub> -C <sub>10</sub>	2.8	600	10
ITI 044.250	A <sub>08</sub> -A <sub>10</sub> ; B <sub>08</sub> -B <sub>10</sub> ; C <sub>08</sub> -C <sub>10</sub>	3.5	500	10
ITI 044.254	A <sub>08</sub> -A <sub>10</sub> ; B <sub>08</sub> -B <sub>10</sub> ; C <sub>08</sub> -C <sub>10</sub>	4.2	400	10
ITI RN4810	A <sub>08</sub> ; B <sub>08</sub> ; C <sub>08</sub>	4.8	12	15
ITI RN4810	A <sub>09</sub> -A <sub>10</sub> ; B <sub>09</sub> -B <sub>10</sub> ; C <sub>09</sub> -C <sub>10</sub>	4.8	15	18.75
DIO DHI 2010SM	A <sub>11</sub> -A <sub>12</sub> ; B <sub>11</sub> -B <sub>12</sub> ; C <sub>11</sub> -C <sub>12</sub>	2.0	1000	10
DIO SDS 2710M	A <sub>11</sub> -A <sub>12</sub> ; B <sub>11</sub> -B <sub>12</sub> ; C <sub>11</sub> -C <sub>12</sub>	3.5	1000	10
DIO DTS 4110M	A <sub>11</sub> -A <sub>12</sub> ; B <sub>11</sub> -B <sub>12</sub> ; C <sub>11</sub> -C <sub>12</sub>	4.0	1000	10
DIO DTS 4510M	A <sub>11</sub> -A <sub>12</sub> ; B <sub>11</sub> -B <sub>12</sub> ; C <sub>11</sub> -C <sub>12</sub>	4.4	1000	10
DIO DTI 5010SM	A <sub>11</sub> -A <sub>12</sub> ; B <sub>11</sub> -B <sub>12</sub> ; C <sub>11</sub> -C <sub>12</sub>	4.9	800	10
DIO SFR5010	A <sub>11</sub> -A <sub>12</sub> ; B <sub>11</sub> -B <sub>12</sub> ; C <sub>11</sub> -C <sub>12</sub>	5.0	15	12

by three influence factors: bone quality, implant geometry and surgical methods, there is no doubt that the predicted model we established with the relatively high accuracy.

#### 4 Conclusions

In this research, a mechanical model was established for the insertion torque of dental implant. The effect of bone quality, the surgical method and the implant geometry were explained by the model parameters: ① bone-quality coefficients, ② insertion speed, and ③ radial

engagement  $h_p$ , chip load  $A$  and implant diameter  $r_p$ , respectively. The more specific conclusions can be drawn as follows:

- (1) The bone-quality coefficients were determined by bone CT value and different in implants with or without cutting edges. The reasonable explanation for this may be the bone quality depended not only on bone density, i.e., bone CT value, but also the microstructure of trabecular bone.

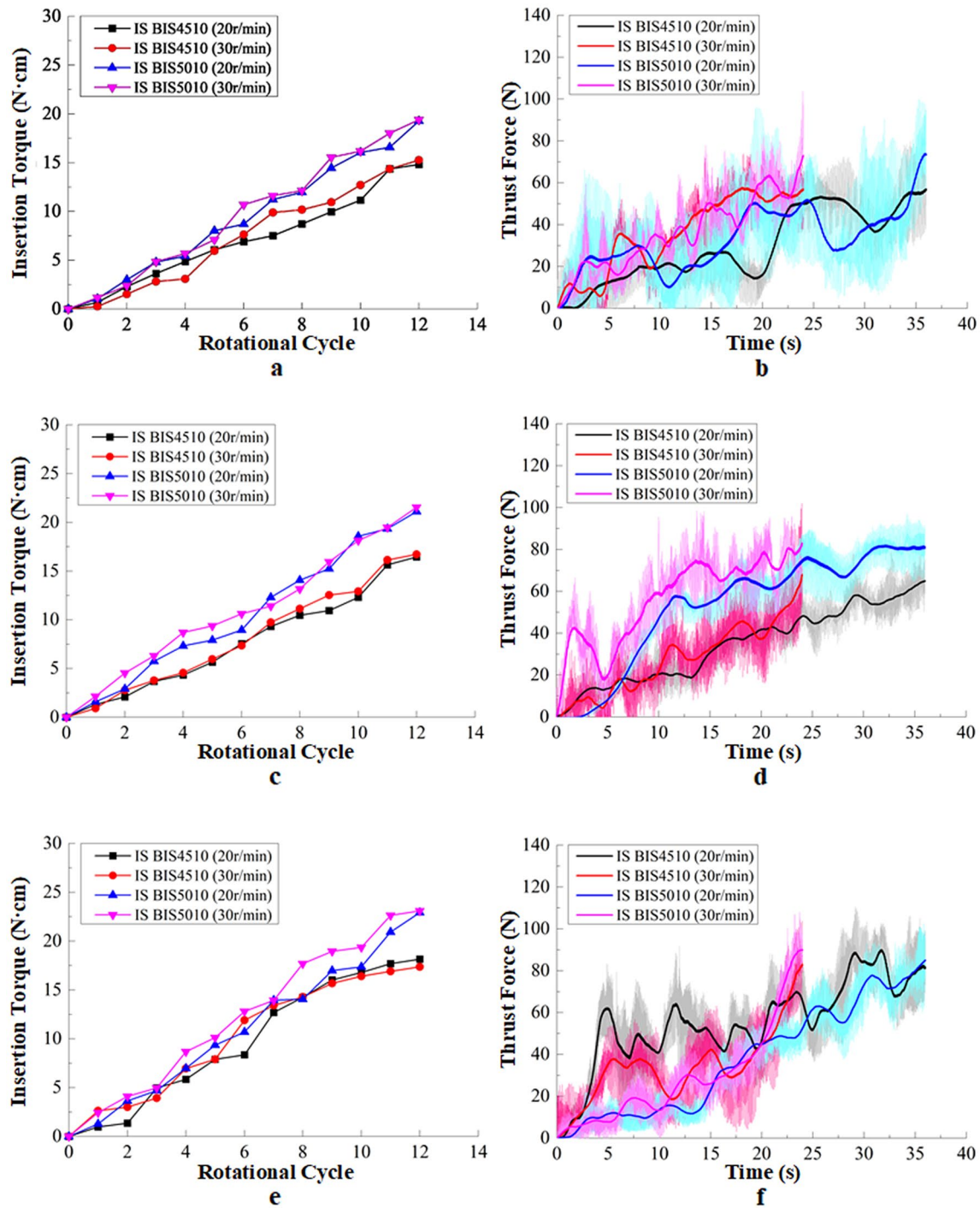


**Figure 6** The insertion torques and thrust forces obtained by insertion experiments: **a–f** data of IS implants, **a** and **b**, **c** and **d**, **e** and **f** were insertion torques and thrust forces of 235–245Hu, 345–355 Hu and 415–425 Hu, respectively; **g–l** data of ITI implants, **g** and **h**, **i** and **j**, **k** and **l** were insertion torques and thrust forces of 235–245Hu, 345–355 Hu and 415–425 Hu, respectively

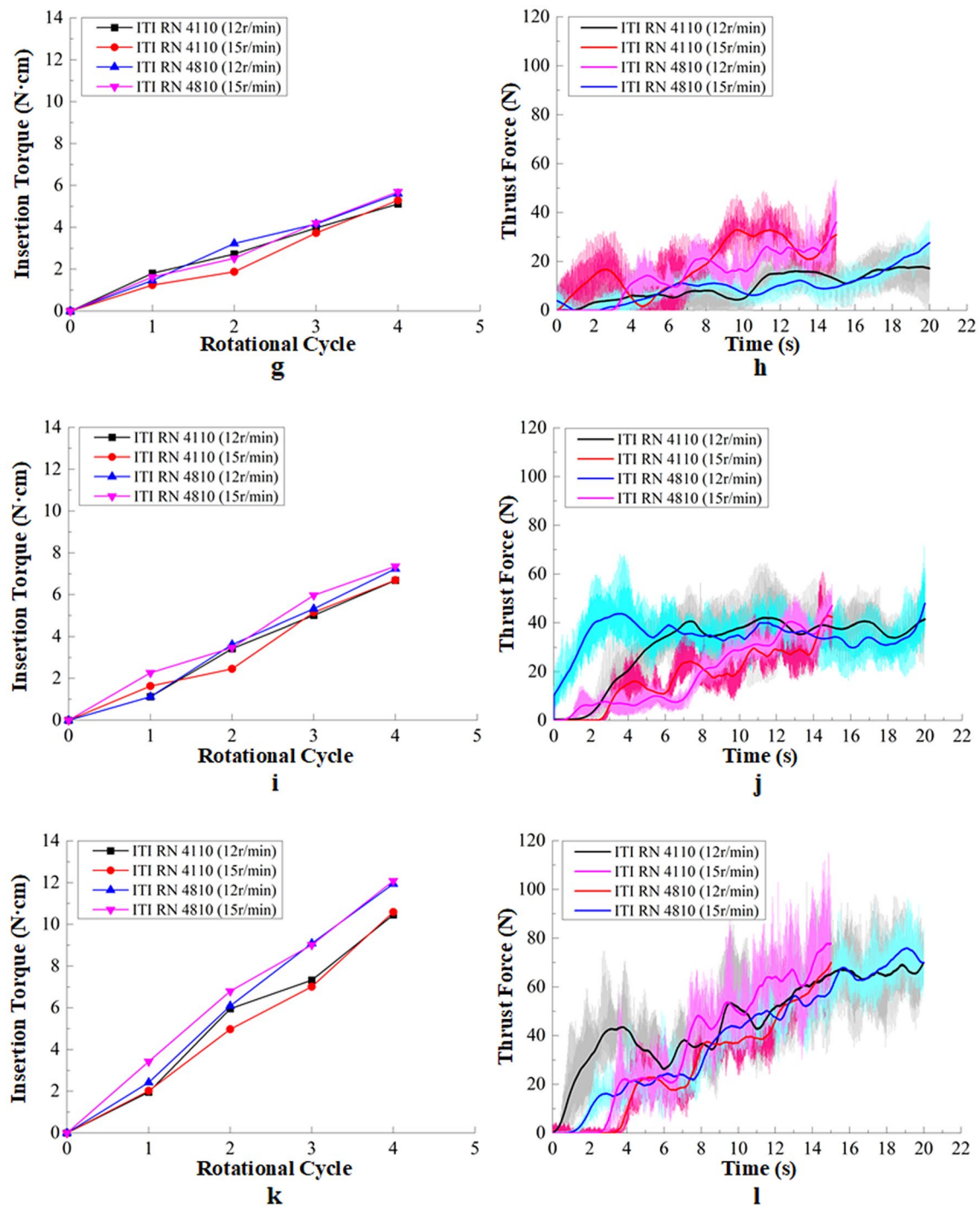


Figure 6 continued

- (2) The error of this mechanical model result from the ① the simplification of modeling; ② the ignored effects of local anisotropy and heterogeneous of bone quality; ③ the surgical errors.
- (3) The established mechanical model can help dentists to make accurate assessment whether the implants and surgical methods are reasonable for individual. Comparing to the fitting formulas, this method can

Table 4 Bone-quality coefficients for thread-cutting

Group	$a_0$	$a_1$	$a_2$	$a_3$	$b_0$	$b_1$	$b_2$	$b_3$
1	14.6	0.17	0.44	0.03	12.9	0.02	0.17	0.003
2	16.7	0.37	0.77	0.07	13.2	0.02	0.18	0
3	58.1	4.81	8.19	0.86	52.8	4.43	7.29	0.795

Table 5 Bone-quality coefficients for thread-forming

Group	$c_0$	$c_1$	$c_2$	$c_3$	$d_0$	$d_1$	$d_2$	$d_3$
1	22.4	0.06	0.16	0	21.2	0.06	0.15	0
2	27.3	0.57	0.82	0.07	26.1	0.57	0.82	0.07
3	60.4	3.87	6.86	0.68	59.2	3.87	6.86	0.68

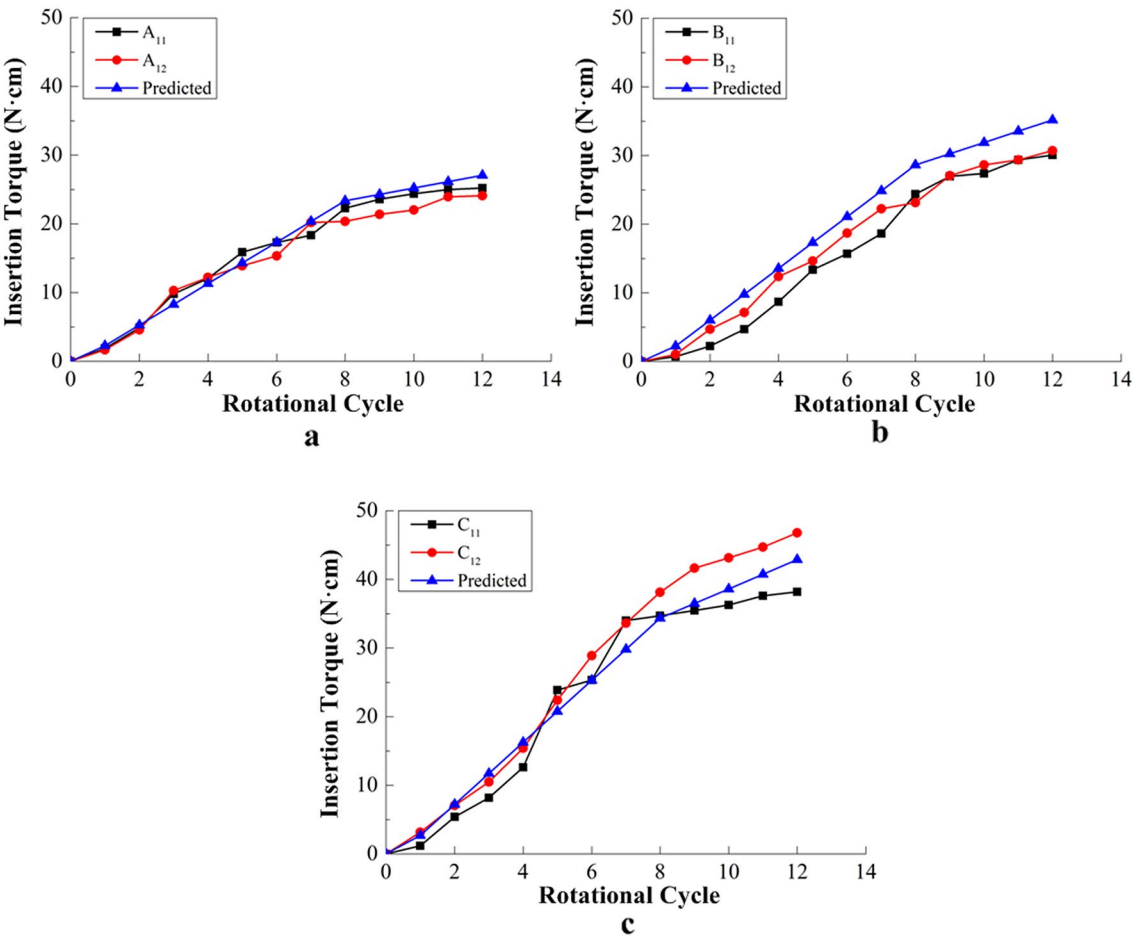


Figure 7 Insertion torques obtained by the mechanical model and experiments: a–c the results of three insertion tests, where A<sub>11</sub>, A<sub>12</sub>, B<sub>11</sub>, B<sub>12</sub>, C<sub>11</sub>, C<sub>12</sub> are the measured values

**Table 6** Comparison of averaged insertion torques from experiments and predictions

Thread number	Group 1			Group 2			Group 3		
	Measured (N·cm)		Pred (N·cm)	Measured (N·cm)		Pred (N·cm)	Measured (N·cm)		Pred (N·cm)
1	1.899	1.669	2.256	0.693	1.036	2.244	1.167	3.158	2.693
2	4.872	4.559	5.270	2.237	4.693	6.012	5.394	7.061	7.214
3	9.805	10.272	8.284	4.693	7.125	9.779	8.171	10.475	11.735
4	12.050	12.197	11.298	8.693	12.362	13.547	12.617	15.392	16.256
5	15.874	13.893	14.312	13.369	14.639	17.314	23.872	22.389	20.777
6	17.274	15.325	17.326	15.693	18.693	21.082	25.349	28.869	25.298
7	18.326	20.186	20.340	18.639	22.237	24.849	33.995	33.612	29.819
8	22.264	20.362	23.354	24.363	23.140	28.617	34.693	38.118	34.34
9	23.592	21.369	24.279	26.964	27.063	30.256	35.460	41.636	36.471
10	24.362	22.012	25.206	27.365	28.634	31.895	36.256	43.124	38.602
11	24.982	23.937	26.132	29.369	29.363	33.534	37.596	44.691	40.733
12	25.193	24.102	27.058	30.069	31.693	35.174	38.172	46.786	42.864
error	7.4%	12.3%	0	16.9%	10.9%	0	12.4%	8.4%	0

avoid plenty of experiments caused by changing implants and surgical method.

#### Acknowledgements

The authors sincerely thanks to Professor Feng Jiang of Huaqiao University for his kindness help and critical discussion during experiment preparation.

#### Author contributions

SZ was in charge of the whole trial; LL wrote the manuscript; LL, QL, CB, AZ assisted with sampling and laboratory analyses. All authors have read and approved the final manuscript.

#### Authors' information

Luli Li, received her master degree from *Shandong University, China*, in 2019. Her research interests include dental implant and bone mechanics. E-mail: sdboll@163.com  
Song Zhang, received his PhD degree from *Shandong University, China*, in 2004. He is currently a professor and doctoral supervisor at *School of Mechanical Engineering, Shandong University, China*. His research fields are fundamental mechanism of high-efficiency cutting and machined surface integrity, biomechanics, and so on.  
Tel: +86-531-88392746; E-mail: zhangsong@sdu.edu.cn  
Quhao Li, received his PhD degree from *Dalian University of Technology, China*, in 2017. He is currently a lecture at *School of Mechanical Engineering, Shandong University, China*. His research interests include computational solid mechanics, numerical simulation. E-mail: quhaoli@sdu.edu.cn  
Cuirong Bian, received her M.M. degree from *Shandong University, China*, in 2004. She is currently a Professor and a chief physician at Department of Prosthodontics, *Qilu Hospital of Shandong University, China*. Her research fields are fixed porcelain repair, reconstruction of maxillofacial bone defects, implant surgery and design, design and fabrication of denture, and so on. E-mail: cuirong\_b88@163.com  
Airong Zhang, received her PhD degree from *Shandong University, China*, in 2020. Her research interests include bone mechanics, dental implant and numerical simulation of bone tissue.  
E-mail: zhangar\_ll@163.com

#### Funding

Supported by Major Research & Development Program of Shandong Province (Grant No. 2015GGX103043), and Taishan Scholars Program of Shandong Province (Grant No. ts201712002).

#### Competing interests

The authors declare no competing financial interests.

#### Author Details

<sup>1</sup>School of Mechanical Engineering, Shandong University, Jinan 250061, China. <sup>2</sup>Key Laboratory of High-efficiency and Clean Mechanical Manufacture of Ministry of Education, Jinan, China. <sup>3</sup>Department of Prosthodontics, Qilu Hospital of Shandong University, Jinan 250012, China.

Received: 24 November 2020 Revised: 4 April 2022 Accepted: 15 April 2022

Published online: 25 May 2022

#### References

- [1] T Irinakis, C Wiebe. Initial torque stability of a new bone condensing dental implant. A cohort study of 140 consecutively placed implants. *Journal of Oral Implantology*, 2009, 35(6): 277–282.
- [2] A Nappo, C Rengo, G Pantaleo, et al. Influence of implant dimensions and position on implant stability: A prospective clinical study in maxilla using resonance frequency analysis. *Applied Science-Basel*, 2019, 9(5): 43–54.
- [3] M Aglietta, V Siciliano, M Zwahlen, et al. A systematic review of the survival and complication rates of implant supported fixed dental prostheses with cantilever extensions after an observation period of at least 5 years. *Clinical Oral Implants Research*, 2009, 20(5): 441–451.
- [4] N Rizkallah, Fischer S, Kraut R A. Correlation between insertion torque and survival rates in immediately loaded implants in the maxilla: A retrospective study. *Implant Dentistry*, 2013, 22(3): 250–254.
- [5] M Akkocaoglu, M C Cehreli, I Tekdemir, et al. Primary stability of simultaneously placed dental implants in extraoral donor graft sites: A human cadaver study. *Journal of the American Association of Oral & Maxillofacial Surgeon*, 2007, 65(3): 400–407.
- [6] P Trisi, G Peretti, E Baldoni, et al. Implant micromotion is related to peak insertion torque and bone density. *Clinical Oral Implants Research*, 2009, 20(5): 467–471.
- [7] S A Lim, J Y Cha, C J Hwang. Insertion torque of orthodontic miniscrews according to changes in shape, diameter and length. *Angle Orthodontist*, 2008, 75(2): 234–240.
- [8] A C Freitas, E A Bonfante, G Giro, et al. The effect of implant design on insertion torque and immediate micromotion. *Clinical Oral Implants Research*, 2015, 23(1): 113–118.



- [9] I Nikellis, P Levi, M Nicolopoulos, et al. Immediate loading of 190 endosseous dental implants: A prospective observational study of 40 patient treatments with up to 2-year data. *International Journal of Oral & Maxillofacial Implants*, 2004, 19(1): 116–123.
- [10] B Wilmes, Y Y Su, D Drescher. Insertion angle impact on primary stability of orthodontic mini-implants. *The Angle Orthodontist*, 2008, 78(6): 1065–1070.
- [11] P S D Patel, D E T Shepherd, D W L Hukins. The effect of screw insertion angle and thread type on the pullout strength of bone screws in normal and osteoporotic cancellous bone models. *Medical Engineering & Physics*, 2010, 32(8): 822–828.
- [12] B Wilmes, D Drescher. Impact of bone quality, implant type, and implantation site preparation on insertion torques of mini-implants used for orthodontic anchorage. *International Journal of Oral and Maxillofacial Surgery*, 2011, 40(7): 697–703.
- [13] J Sakoh, U Wahlmann, E Stender, et al. Primary stability of a conical implant and a hybrid, cylindrical screw-type implant in vitro. *International Journal of Oral & Maxillofacial Implants*, 2006, 21(4): 560–566.
- [14] C N Elias, F A Rocha, A L Nascimento, et al. Influence of implant shape, surface morphology, surgical technique and bone quality on the primary stability of dental implants. *Journal of the Mechanical Behavior of Biomedical Materials*, 2012, 16:169–180.
- [15] M M Shalabi, J G C Wolke, J A Jansen. The effects of implant surface roughness and surgical technique on implant fixation in an in vitro model. *Clinical Oral Implants Research*, 2006, 17(2): 172–178.
- [16] C Makary, A Rebaudi, G Sammartino, et al. Implant primary stability determined by resonance frequency analysis: correlation with insertion torque, histologic bone volume, and torsional stability at 6 weeks. *Implant Dentistry*, 2012, 21(6): 474–480.
- [17] I Turkyilmaz, C Tumer, E N Ozbek, et al. Relations between the bone density values from computerized tomography, and implant stability parameters: a clinical study of 230 regular platform implants. *Journal of Clinical Periodontology*, 2007, 34(8): 716–722.
- [18] T M Keaveny, E F Morgan, G L Niebur, et al. Biomechanics of trabecular bone. *Annual Review of Biomedical Engineering*, 2001, 3(1): 307–333.
- [19] A Beer, A Gahleitner, A Holm, et al. Correlation of insertion torques with bone mineral density from dental quantitative CT in the mandible. *Clinical Oral Implants Research*, 2003, 14(5): 616–620.
- [20] O Ozan, K Orhan, I Turkyilmaz. Correlation between bone density and angular deviation of implants placed using CT-generated surgical guides. *Journal of Craniofacial Surgery*, 2011, 22(5): 1755–1761.
- [21] J H Lee, J W Park, J H Lee, et al. The correlation between insertion torque of pedicle screws with bone mineral density values in posterior lumbar pedicle screw fixation. *The Spine Journal*, 2011, 11(10): S145–S146.
- [22] J S Agapiou. Evaluation of the effect of high speed machining on tapping. *Journal of Engineering for Industry* 1994, 116(4): 457–462.
- [23] G Fromentin, G Poulachon, A Moisan, et al. Precision and surface integrity of threads obtained by form tapping. *CIRP Annals*, 2005, 54(1): 519–522.
- [24] T Cao, J W Sutherland. Investigation of thread tapping load characteristics through mechanistics modeling and experimentation. *International Journal of Machine Tools and Manufacture*, 2002, 42(14): 1527–1538.
- [25] A P S Dogra, S G Kapoor, R E DeVor. Mechanistic model for tapping process with emphasis on process faults and hole geometry. *Journal of Manufacturing Science and Engineering*, 2002, 124(1): 18–25.
- [26] J E Lee, B A Gozen, O B Ozdoganlar. Modeling and experimentation of bone drilling forces. *Journal of Biomechanics*, 2012, 45(6): 1076–1083.
- [27] F Jiang, T Zhang, L Yan. Analytical model of milling forces based on time-variant sculptured shear surface. *International Journal of Mechanical Sciences*, 2016, 115: 190–201.
- [28] A Moufki, D Dudzinski, A Molinari, et al. Thermoviscoplastic modelling of oblique cutting: forces and chip flow predictions. *International Journal of Mechanical Sciences*, 2000, 42(6): 1205–1232.
- [29] X W Liu, K Cheng, D Webb, et al. Improved dynamic cutting force model in peripheral milling. Part I: Theoretical model and simulation. *The International Journal of Advanced Manufacturing Technology*, 2002, 20(9): 631–638.
- [30] S Chowdhary, R E Devor, S G Kapoor. Modeling forces including elastic recovery for internal thread forming. *Journal of Manufacturing Science and Engineering*, 2003, 125(4): 681–688.

**Submit your manuscript to a SpringerOpen<sup>®</sup> journal and benefit from:**

- Convenient online submission
- Rigorous peer review
- Open access: articles freely available online
- High visibility within the field
- Retaining the copyright to your article

---

Submit your next manuscript at ► [springeropen.com](https://www.springeropen.com)